

Lanthanum-doped zinc borate glasses: fabrication, structural analysis, thermal properties, and gamma radiation shielding performance

Yu. S. Hordieiev *, A. V. Zaichuk

Ukrainian State University of Science and Technologies, 8 Haharina Avenue, Dnipro, 49005, Ukraine

Zinc borate glasses with a composition formula of $(60-m)\text{B}_2\text{O}_3-40\text{ZnO}-m\text{La}_2\text{O}_3$ ($m = 0, 3, 6, 9, 12,$ and 15 mol%) were synthesized via the melt-quenching technique for the purpose of investigating the effects of La_2O_3 incorporation on their structural, thermal, and radiation shielding properties. Amorphous structures for all samples (coded as ZBLa0 to ZBLa15) were confirmed using X-ray diffraction and Differential thermal analysis. Incorporating La_2O_3 significantly influenced the glass matrix, increasing density, molar volume, thermal expansion and the glass transition, while decreasing the crystallization peak temperature and thermal stability. These effects highlight La_2O_3 's role as a network modifier that depolymerizes the glass structure, as indicated by shifts in FT-IR bands and altered vibrational modes. Radiation shielding properties improve markedly with La_2O_3 addition, as evidenced by increased mass attenuation coefficients and effective atomic numbers, making the glass with 15 mol% La_2O_3 (ZBLa15) particularly effective at gamma-ray attenuation across a wide photon energy range. These findings suggest that La_2O_3 -doped zinc borate glasses are highly suitable for applications requiring enhanced radiation shielding alongside reliable thermal performance.

(Received November 14, 2024; Accepted February 4, 2025)

Keywords: Zinc borate glasses, Structure, Glass stability, Radiation shielding properties, Thermal expansion

1. Introduction

In recent times, borate glass matrices have emerged as an area of intense research interest due to their distinctive physical characteristics, including exceptional transparency, thermal resilience, low melting temperature, and robust glass-forming abilities [1, 2]. These properties render borate glasses valuable in a multitude of applications, spanning from optoelectronic devices for biomedical applications to advanced electronic systems and radiation shielding materials [3, 4]. Given their versatility, there is a growing focus on exploring and enhancing the physical properties of borate glasses to extend their usability across various technological fields.

Particularly notable within this category are zinc borate glasses, which are of particular interest due to zinc oxide's dual role in these structures [3]. ZnO can function either as a network modifier, disrupting boron-oxygen-boron bonds and creating non-bridging oxygen (NBO) and defects, or as a network former, integrating into the glass structure through ZnO_4 units [5]. This structural adaptability enhances the mechanical strength, chemical durability, and thermal stability of zinc borate glasses, making them highly desirable for applications requiring a blend of transparency and durability.

The functionality of borate glasses extends further with the integration of rare-earth elements like lanthanum oxide (La_2O_3). Lanthanum oxide, known for enhancing glass density and stability, contributes to the overall performance of the glass, especially under conditions where radiation protection and durability are essential [6, 7]. Such doped glasses are also appealing for applications that require chemical stability and improved mechanical properties. The adaptability of borate-based glasses, when considered in conjunction with the synergistic effects of ZnO and La_2O_3 , has facilitated the development of materials that are well-suited for demanding

* Corresponding author: yuriihordieiev@gmail.com
<https://doi.org/10.15251/JOR.2025.211.85>

technological applications [8]. These range from optoelectronic devices and radiation shielding materials to advanced photonic components and nonlinear optical devices. Furthermore, lanthanum doping in zinc borate glasses shows promise in biomedical fields and energy-related technologies, owing to its potential for enhancing radiation protection and durability. With ongoing research aimed at fine-tuning these materials for specific uses, lanthanum-doped zinc borate glasses are positioned as versatile candidates in both established and emerging fields of science and industry. This study investigates how La_2O_3 doping impacts zinc borate glass characteristics, emphasizing their potential as next-generation materials for diverse high-performance applications.

2. Materials and methods

The chemical compositions and designations of the different glass samples investigated in the present investigation are given in Table 1. ZBLa glasses were synthesized using a well-established melt-quench technique, with a chemical formula $(60-m)\text{B}_2\text{O}_3-40\text{ZnO}-m\text{La}_2\text{O}_3$, where the variable m ranges between 0 and 15 mol%, allowing for a comprehensive investigation of the incorporation of La_2O_3 into the glass structure. The samples are designated as ZBLa0, ZBLa3, ZBLa6, ZBLa9, ZBLa12, and ZBLa15, corresponding to La_2O_3 contents of 0, 3, 6, 9, 12, and 15 mol%, respectively. For the glass preparation, we employed high-purity raw materials: ZnO (99.7%, Reachim), H_3BO_3 (99.9%, Reachim), and La_2O_3 (99.9%, Sigma-Aldrich). These materials were precisely weighed and thoroughly mixed to ensure homogeneity. The prepared batch was melted in a 60 mL corundum crucible using a high-temperature furnace (Nabertherm LHTCT 01/16) equipped with SiC rod heating elements. The melting process was conducted at 1350°C for one hour to achieve complete fusion and uniformity. The cast ZBLa samples underwent an annealing process in a muffle furnace (SNOL 7.2/900) at 590°C for a period of five hours to release any internal stresses [9]. The glasses were then allowed to cool to the ambient temperature at a controlled rate of 50°C per hour [10].

Table 1. Comprehensive glass chemical composition (mol%), along with physical and thermal property data for ZBLa glasses.

Glass code	Glass composition			Density, $[\text{g}/\text{cm}^3]$	Molar volume, $[\text{cm}^3/\text{mol}]$	Dilatometry results			Stability parameters	
	B_2O_3	ZnO	La_2O_3			CTE, $[\text{ppm}/^\circ\text{C}]$	T_g , $^\circ\text{C}$	T_d , $^\circ\text{C}$	ΔT , $^\circ\text{C}$	C_{SP}
ZBLa0	60	40	0	3.030	24.5	4.70	570	597	216	12.88
ZBLa3	57	40	3	3.217	25.5	4.82	580	606	205	15.69
ZBLa6	54	40	6	3.424	26.2	5.08	587	611	182	13.71
ZBLa9	51	40	9	3.592	27.2	5.47	591	614	162	12.63
ZBLa12	48	40	12	3.805	27.7	5.72	593	618	146	11.06
ZBLa15	45	40	15	4.024	28.1	6.34	595	621	129	7.96

Thermal behavior was rigorously examined using differential thermal analysis (DTA) with a Q-1500 Paulik-Paulik-Erdey Derivatograf (Hungary) in platinum crucibles. $\alpha\text{-Al}_2\text{O}_3$ (99.9%, Thermo Fisher) served as a reference material to ensure precision [9]. The heating protocol involved a constant rate of $5^\circ\text{C}/\text{min}$ [10]. Key thermal events were identified from the DTA plots: the glass transition (T_g) at the first endothermic shift, the onset of crystallization (T_x) at the initial exothermic change, and the peak crystallization temperature (T_p) at the maximum of the exothermic peak. To investigate any crystalline phases that may have formed, the powder was heated at T_p for five hours and subsequently analyzed using XRD with a Bruker D8 diffractometer (Co-K α source, $\lambda_{\text{avg}} = 1.7902 \text{ \AA}$). Additionally, the morphology of the crystalline phases in the ZBLa samples was studied using a FE-SEM MIRA 3 LMU, providing insight into the structural characteristics post-crystallization.

Infrared spectra were acquired using a FT-IR Spectrometer (iS10 Nicolet), spanning 1600 to 400 cm^{-1} with 2 cm^{-1} resolution, utilizing the KBr pellet method. Additional measurements included thermal properties such as thermal expansion and glass density using a dilatometer and the Archimedes principle, with meticulous attention to accuracy and repeatability. Additionally, critical determinations of radiation shielding characteristics like the mass/linear attenuation coefficient (MAC/LAC), effective atomic number (Z_{eff}), mean free path and half-value layer were calculated for ZBLa glasses across a gamma-ray energy spectrum of 15 keV to 15 MeV, utilizing the Phy-X/Photon Shielding and Dosimetry software developed by Şakar et al. [11]. This extensive evaluation is vital for determining the interaction of high-energy gamma photons with these glass materials, which plays an essential role in the development of new glass types for radiation shielding in various medical and technological applications [12].

3. Results and discussion

The XRD patterns shown in Figure 1a illustrate the structural characteristics of the prepared ZBLa glass samples across a 2-theta range between 10 and 90 degrees. The broad hump observed in the XRD patterns around the 25°–45° range, in conjunction with the absence of sharp peaks, clearly differentiates these amorphous glass samples from crystalline substances, underscoring their fundamentally different atomic arrangements.

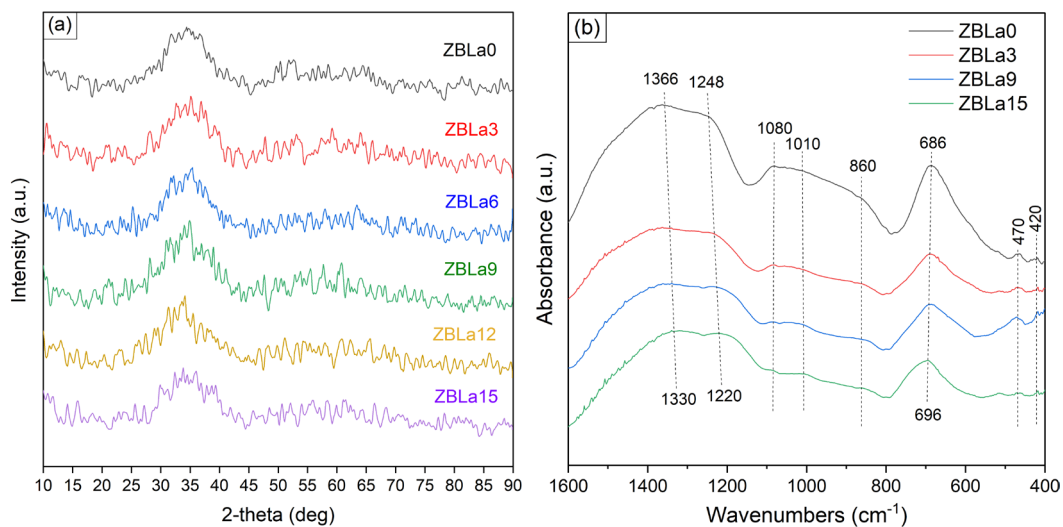


Fig. 1. XRD (a) and FT-IR (b) results of ZBLa glasses.

To examine the structural alterations caused by incorporating La_2O_3 into a $60\text{B}_2\text{O}_3\text{--}40\text{ZnO}$ glass matrix, we focused on the mid-IR region ($400\text{--}1600\text{ cm}^{-1}$), where zinc borate glass vibrational modes are active. The study reveals that La_2O_3 significantly alters the glass's local structure (Fig. 1b), as evidenced by changes in the intensities of three main absorption bands (690 , $800\text{--}1100$, and $1150\text{--}1450\text{ cm}^{-1}$), which correspond to vibrations of specific structural groups within the borate matrix. Significantly, the pronounced absorption band at 1366 cm^{-1} is associated with the stretching vibrations of non-bridging B--O^- bonds present in metaborate units, designated as BO_2^- [13, 14], where O represents bridging oxygen. Furthermore, the strong peak at 1248 cm^{-1} can be attributed to the asymmetric stretching vibrations of BO_3 triangular units [15, 16]. These units form part of complex ring-type superstructures, including boroxol rings and tri-, tetra-, and pentaborate formations [13]. The presence of La_2O_3 shifts these bands to lower wavenumbers, indicating a reduction in the polymerization degree of the borate network. The spectral region from about 800 to 1100 cm^{-1} shows a reduction in absorption intensity with increased La_2O_3

concentration, likely due to a reduced presence of structures containing tetrahedrally coordinated boron, which absorb infrared light at specific wavelengths (860, 1010, and 1080 cm^{-1}). This observation aligns with previous studies [14], which noted the disintegration of large borate groups containing tetrahedral boron as the network becomes increasingly modified. Additionally, a broad band between 600–800 cm^{-1} is attributed to the bending modes of trigonal borate groups [14], which shift from 686 cm^{-1} to 696 cm^{-1} as non-bridging oxygen (NBO) content increases at these sites. Recent studies, such as those by Azooz et al. [17], have also identified a far-infrared band near 470 cm^{-1} as indicative of ZnO_4 units in $\text{ZnO}(50\text{--}75\text{ mol}\%)\text{--B}_2\text{O}_3$ glasses. The low-frequency band at about 420 cm^{-1} in our spectra can be attributed to vibrations of Zn^{2+} cations [17, 18].

DTA is a pivotal analytical method used to study the thermal behavior of materials, including glasses, by revealing how they respond to temperature changes. DTA plots in Figure 2 show the thermal behavior of a $60\text{B}_2\text{O}_3\text{--}40\text{ZnO}$ glass with increasing amounts of La_2O_3 , where B_2O_3 is progressively substituted by La_2O_3 in the range of 0 to 15 mol%. As La_2O_3 is introduced and increased in the glass matrix, several changes in the thermal properties are observed. For the base composition (ZBLa0), the T_g is around 570°C, and as La_2O_3 is added, T_g increases steadily, reaching around 600°C at 15 mol% La_2O_3 . This suggests that introducing La_2O_3 into the zinc borate glass matrix increases the structural rigidity. As the La_2O_3 content increases, there is a shift in the crystallization peaks towards lower temperatures. For the ZBLa0 glass without La_2O_3 , the crystallization peak (T_p) appears prominently around 820°C. However, as La_2O_3 is introduced, T_p shifts gradually lower, indicating that the glass becomes more prone to crystallization at lower temperatures. This is seen clearly in the case of the ZBLa15 glass with 15 mol% La_2O_3 , where the crystallization peak occurs at approximately 766°C. The decrease in crystallization temperature suggests that La_2O_3 reduces the thermal stability of the zinc borate glass. The overall shape of the crystallization peak remains relatively sharp, but with higher La_2O_3 content, the intensity decreases, indicating less pronounced crystallization or a change in the crystalline phases formed.

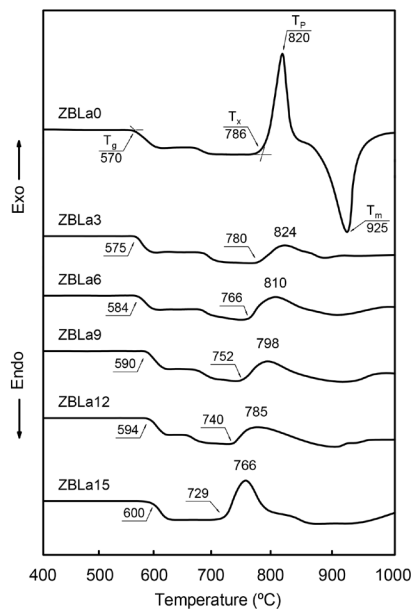


Fig. 2. DTA thermograms of ZBLa glasses.

The XRD patterns (Fig. 3) for the crystallized glass samples (ZBLa0, ZBLa9, and ZBLa15) in the figure illustrate the impact of substituting B_2O_3 with La_2O_3 on the crystallization phases. For the ZBLa0 sample (black), the major crystalline phases observed are $\text{Zn}_4\text{B}_6\text{O}_{13}$ (PDF 01-083-2426) and ZnB_4O_7 (PDF 01-071-0634). When La_2O_3 is introduced (ZBLa9, red curve), the same $\text{Zn}_4\text{B}_6\text{O}_{13}$ and ZnB_4O_7 phases are still dominant, but the intensity of peaks suggests a modification in crystallinity or phase distribution. In the ZBLa15 sample (blue), the introduction

of 15 mol% La_2O_3 leads to the formation of a new phase, LaBO_3 (PDF 01-076-1389), which is confirmed by the corresponding peaks in the XRD pattern. The gradual replacement of B_2O_3 with La_2O_3 affects the phase composition, favoring LaBO_3 formation.

The SEM images (Fig.3, right panel) support the XRD findings, showing the microstructural changes caused by the introduction of La_2O_3 . In the sample without La_2O_3 (Fig.3a), the structure is characterized by well-formed, faceted crystals. When 9 mol% La_2O_3 is introduced (Fig.3b), the crystals are smaller and appear more fragmented, suggesting that the La_2O_3 addition affects the crystal growth process. At 15 mol% La_2O_3 (Fig.3c), the sample exhibits more complex structures with larger, needle-like or elongated crystalline forms, indicating that higher La_2O_3 content promotes the formation of a different microstructure, likely due to the dominance of LaBO_3 crystallization.

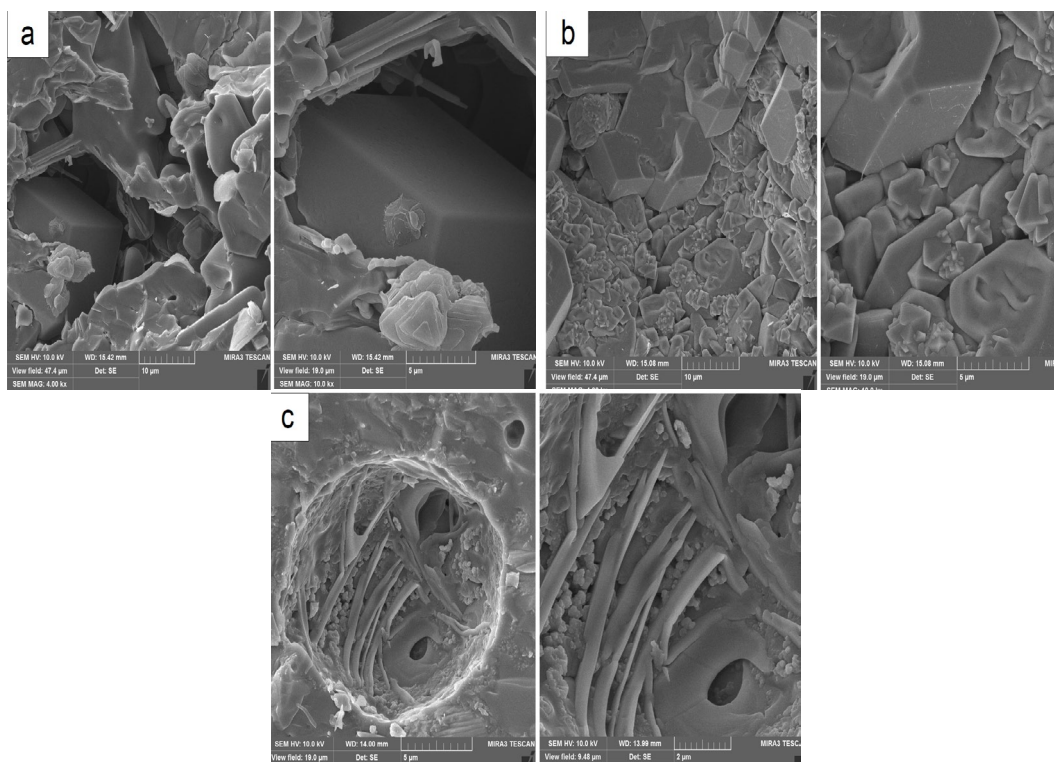
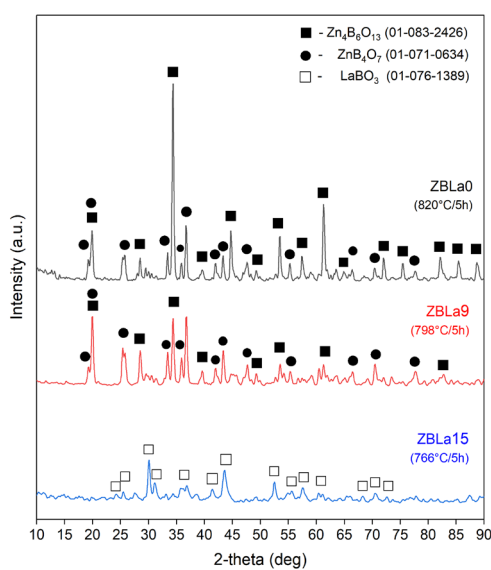


Fig. 3. XRD and SEM analyses of the ZBLa0 (a), ZBLa9 (b), and ZBLa15 (c) samples.

Glass stability, one of the main determinants of a glass's resistance to devitrification during heating, is assessed using parameters such as $\Delta T = T_x - T_g$ (Dietzel criterion) [19] and $C_{SP} = [(T_p - T_x) \times \Delta T] / T_g$ (Saad-Poulain criterion) [20]. In this study, ΔT decreases significantly from 216°C to 129°C with increasing La_2O_3 content, showing reduced thermal stability. However, the Saad and Poulain criterion, which further evaluates the resistance to devitrification, reveals an improvement in thermal stability at lower La_2O_3 concentrations (3 to 6 mol%), where C_{SP} values increase from 12.88 to 15.69. Further increasing the La_2O_3 content beyond 6 mol% leads to a decrease in C_{SP} , reaching 7.96 at 15 mol% La_2O_3 , indicating diminished stability. Therefore, moderate La_2O_3 content enhances the glass's resistance to crystallization, but excessive amounts lead to reduced thermal stability.

Dilatometric analysis, presented in Figure 4 and summarized in Table 1, was employed to investigate the thermal expansion behavior of the ZBLa glass samples, including the glass softening point (T_d) by dilatometry, the T_g , and the linear coefficient of thermal expansion (CTE) [9]. These parameters are critical for evaluating the suitability of the glass for various applications, as they are intrinsically linked to the glass's chemical composition [10] and thermal response [21]. The CTE, T_g , and T_d values were derived from the dilatometric curves, revealing that all three properties increase progressively with the amount of La_2O_3 added. The T_g values from dilatometry closely align with those from DTA, with minor discrepancies (1–6 °C) attributed to different heating rates during measurements (3 °C/min for dilatometry vs. 5 °C/min for DTA). The observed increase in CTE, from 4.7 to 6.34 ppm/°C, correlates with higher La_2O_3 content, explained by the depolymerization effect of this modifier oxide on the glass network. La_2O_3 acts as a network modifier, disrupting boron-oxygen-boron linkages and forming non-bridging oxygens, which decreases network connectivity and enhances thermal expansion upon heating.

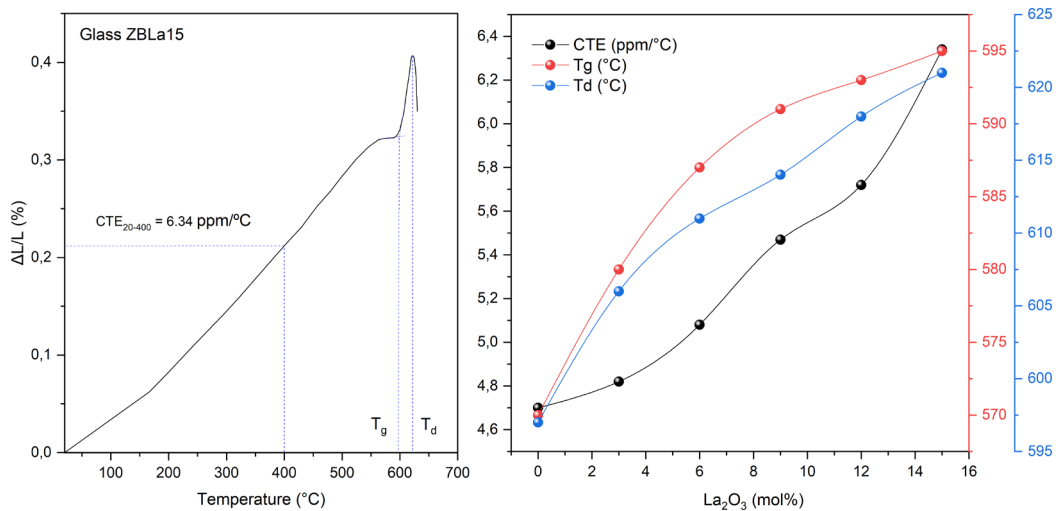


Fig. 4. Dilatometry results of ZBLa glasses.

Further insight into the structural changes in the glass system can be gained by examining important physical quantities involved, such as density (ρ) and molar volume (V_m), which are highly sensitive indicators of changes within the glass structure. As shown in Table 1, the addition of La_2O_3 (0–15 mol%) results in an increase in both ρ and V_m . Specifically, the value of ρ rises substantially from 3.030 to 4.024 g/cm³, while the value of V_m increases from 24.5 to 28.1 cm³/mol. The rise in density is largely attributable to the substitution of the comparatively lightweight B_2O_3 (69.620 g/mol) by the considerably more substantial La_2O_3 (325.809 g/mol). Interestingly, despite the increase in density, the V_m of the glass also increases with the addition of La_2O_3 , which might initially seem counterintuitive. This phenomenon can be explained by considering the ionic radii of the cations involved. La^{3+} ions have a significantly larger ionic radius of approximately 1.22 Å compared to the smaller B^{3+} ions with an ionic radius of about 0.20 Å

[22]. Incorporating the larger La^{3+} ions into the glass network results in the creation of additional free volume and an expansion of the network structure, leading to a decrease in the overall compactness of the resulting glass. This expansion of the glass network is consistent with the depolymerization observed in the FT-IR analysis, where the formation of NBOs and the alteration of BO_4 units to BO_3 units [23, 24] contribute to a less interconnected and more open glass structure. This concurrent rise in both density and molar volume has also been reported in other studies investigating the effects of La_2O_3 on similar glass systems [6, 25].

Using Phy-X/PSD software [11], we calculated the mass (MAC) and linear (LAC) attenuation coefficients [26] across a wide photon energy range (Fig. 5), with the objective of assessing the ZBLa glasses' resilience to ionizing radiation. The results revealed that both MAC and LAC values decrease with increasing photon energy, exhibiting the highest values at lower energies due to the dominance of the photoelectric absorption process [27]. The results, illustrated in Fig. 5a, demonstrate that higher La_2O_3 content leads to increased MAC values. This trend is influenced by the higher molecular mass of La_2O_3 (325.809 g/mol) compared to B_2O_3 (69.620 g/mol) and the increased density of the ZBLa samples with higher La_2O_3 content, which enhances their gamma-ray shielding capability. At low photon energies (0.015 MeV), the MAC values significantly rise – from 29.518 cm^2/g for the La_2O_3 -free glass (ZBLa0) to 44.323 cm^2/g for the glass with the highest La_2O_3 content (ZBLa15) – due to dominant photoelectric absorption. Although MAC values decrease overall at higher energies (15 MeV), they still increase with La_2O_3 content, indicating improved shielding across the energy spectrum. A notable spike in MAC at 0.040 MeV corresponds to the K-absorption edge of lanthanum [28–30], absent in the La_2O_3 -free glass, highlighting the significant role of La_2O_3 in enhancing attenuation. This study underscores that increasing La_2O_3 content in zinc borate glasses substantially improves their gamma-ray attenuation ability, making ZBLa15 the most effective among the proposed glasses for radiation shielding applications. Similarly, the linear attenuation coefficients (Fig. 5b) mirrored the trends observed in MAC, with higher values for glasses containing more La_2O_3 , reinforcing the role of glass composition and density in radiation attenuation.

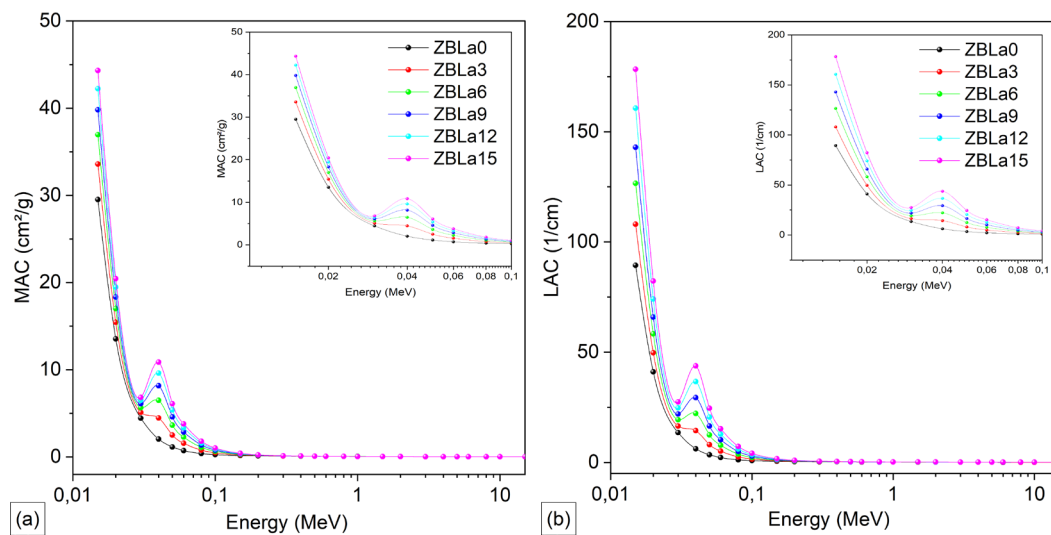


Fig. 5. MAC (a) and LAC (b) of ZBLa glasses

The half-value layer (HVL) along with the mean free path (MFP), both key metrics for evaluating the material thickness required for effective shielding, were also calculated. The values of both HVL and MFP increased with photon energy (see Fig. 6) but decreased with higher La_2O_3 content. For comparison, at 0.015 MeV, the HVL for ZBLa0 was 0.00775 cm, while for ZBLa15 it was 0.00389 cm – a reduction of approximately 49.8%. At 15 MeV, the HVL values increased to 9.869 cm for ZBLa0 and 5.406 cm for ZBLa15, indicating that higher La_2O_3 content significantly improves shielding efficiency even at higher energies. The decrease in HVL and MFP with

increasing La_2O_3 content is primarily due to the inverse relationship between these parameters and the LAC. The higher density of glasses with more La_2O_3 enhances their ability to attenuate gamma rays, making ZBLa15 the most effective of all the ZBLa series glasses for radiation shielding applications.

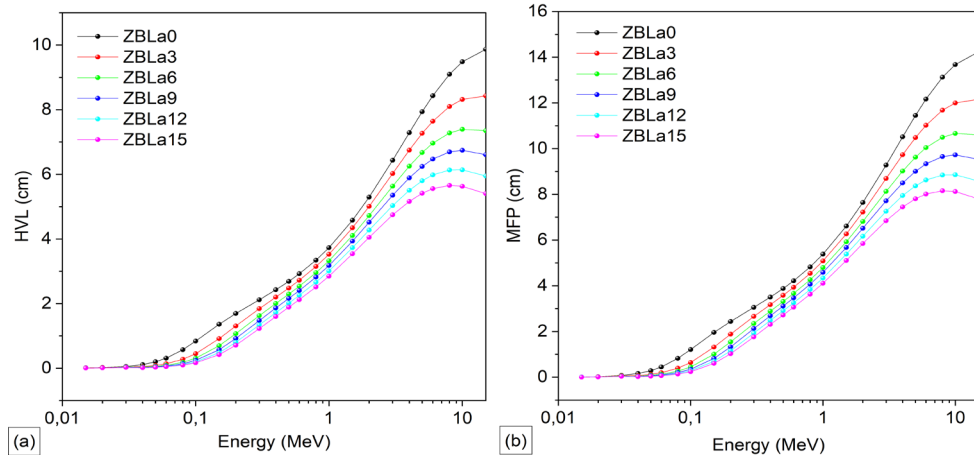


Fig. 6. Changes in HVL (a) and MFP (b) with photon energy for ZBLa glasses containing different concentrations of La_2O_3 .

Furthermore, we evaluated the effective atomic number (Z_{eff}) of the ZBLa glasses to gain deeper insight into their gamma-ray attenuation capabilities. The Z_{eff} is a crucial parameter as it represents a weighted average that reflects the combined contribution of each constituent element within the glass composition to the overall photon attenuation process [31]. In our study of ZBLa glasses, Fig. 7 illustrates that Z_{eff} values exhibit a pronounced dependence on both photon energy and La_2O_3 content. The Z_{eff} values remained relatively stable within the low-energy range of 0.015–0.030 MeV. However, a marked increase was observed at approximately 0.040 MeV, which is attributable to the K-absorption edges of La_2O_3 [32], where photons possess just enough energy to eject inner-shell electrons, thereby enhancing attenuation [33].

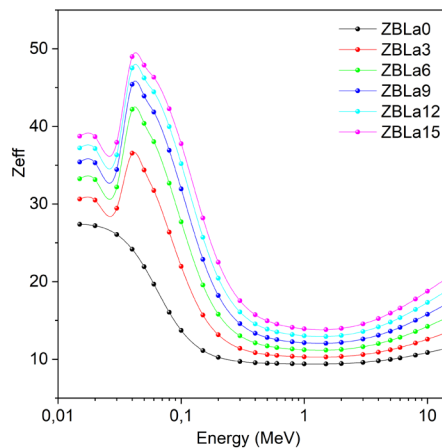


Fig. 7. Z_{eff} of ZBLa glasses.

This is followed by a decline in Z_{eff} from 0.05 to 0.4 MeV as photoelectric interactions decrease. In the intermediate energy range of 0.4 to 5.0 MeV, Z_{eff} stabilizes and becomes relatively insensitive to changes in photon energy. This plateau is indicative of Compton scattering

becoming [34] the predominant interaction mechanism. At higher photon energies, specifically between 5 and 15 MeV, there is a slight rise in Z_{eff} , which is linked to electron-positron pair production caused by interactions between high-energy photons with electrons in the ZBLa glass structure.

The progressive increase in La_2O_3 concentration from 0 to 15 mol% leads to a corresponding rise in Z_{eff} values, indicating better photon attenuation capabilities. For example, at 0.015 MeV, the Z_{eff} for ZBLa15 is 38.74, while for ZBLa0 (with no La_2O_3), it is 27.39. The results show a clear trend: ZBLa15 > ZBLa12 > ZBLa9 > ZBLa6 > ZBLa3 > ZBLa0, confirming that glasses with higher La_2O_3 concentrations are more effective at photon attenuation. This trend is observed across the energy spectrum, with ZBLa15 demonstrating consistent superiority in gamma-ray shielding compared to other compositions, particularly at lower photon energies where the dominance of the photoelectric effect [35] is evident.

4. Conclusions

Incorporating La_2O_3 into the $60\text{B}_2\text{O}_3\text{-}40\text{ZnO}$ glass matrix significantly affects the glasses' structural, thermal, and radiation shielding properties. Fourier Transform Infrared spectroscopy reveals that adding up to 15 mol% La_2O_3 decreases the polymerization degree of the borate network, indicated by shifts in absorption bands to lower wavenumbers. DTA shows an increase in the glass transition temperature from approximately 570°C to 600°C, while the crystallization temperature decreases from about 820°C to 766°C with 15 mol% La_2O_3 , reducing the thermal stability parameter ΔT from 216°C to 129°C. Physical properties like density and molar volume also increased with La_2O_3 content, from 3.030 to 4.024 g/cm³ and 24.5 to 28.1 cm³/mol, respectively, reflecting network depolymerization. The thermal expansion coefficient increased from 4.70 to 6.34 ppm/°C, aligning with the observed structural modifications.

Importantly, the enhanced gamma-ray attenuation properties with higher La_2O_3 content – demonstrated by increased MAC and decreased half-value layers – make these glasses promising candidates for radiation shielding applications. The glass with 15 mol% La_2O_3 (ZBLa15) exhibits the most effective gamma-ray shielding among the studied compositions. This study emphasizes that by modifying the La_2O_3 concentration, the structural, thermal, physical, and radiation shielding features incorporated in zinc borate glasses can be improved, making them suitable for applications in medical, nuclear, and industrial fields requiring robust gamma-ray protection.

References

- [1] M. Bengisu, *Journal of Materials Science* **51**, 2199 (2016); <https://doi.org/10.1007/s10853-015-9537-4>
- [2] V. I. Goleus, Y. S. Hordieiev, A. V. Nosenko, *Voprosy Khimii i Khimicheskoi Tekhnologii* **4**, 92 (2018).
- [3] S. Cetinkaya Colak, I. Akyuz, F. Atay, *Journal of Non-Crystalline Solids* **432**, 406 (2016); <https://doi.org/10.1016/j.jnoncrysol.2015.10.040>
- [4] M. I. Sayyed, M. H. A. Mhareb, Y. S. M. Alajerami, K. A. Mahmoud, M. A. Imheidat, F. Alshahri, M. Alqahtani, T. Al-Abdullah, *Optik* **239**, 166790 (2021); <https://doi.org/10.1016/j.ijleo.2021.166790>
- [5] Y. S. Hordieiev, A. V. Zaichuk, *MRS Advances* **8**, 201 (2023); <https://doi.org/10.1557/s43580-023-00511-7>
- [6] S. A. M. Issa, G. Susoy, A. M. Ali, H. O. Tekin, Y. B. Saddeek, A. Al-Hajry, H. Algarni, P. S. Anjana, O. Agar, *Applied Physics A* **125**, 867 (2019); <https://doi.org/10.1007/s00339-019-3169-5>
- [7] Yu. S. Hordieiev, A. V. Zaichuk, *Journal of Inorganic and Organometallic Polymers and Materials* **33**(2), 591 (2023); <https://doi.org/10.1007/s10904-022-02526-3>
- [8] H. Lin, X. Zhao, W. Chen, L. Luo, *Journal of Alloys and Compounds* **479**, 859–862 (2009); <https://doi.org/10.1016/j.jallcom.2009.01.082>

- [9] Yu. S. Hordieiev, A. V. Zaichuk, Digest Journal of Nanomaterials and Biostructures **19**, 773 (2024); <https://doi.org/10.15251/DJNB.2024.192.773>
- [10] Yu. S. Hordieiev, A.V. Zaichuk, Chalcogenide Letters, **21**(3), 243 (2024); <https://doi.org/10.15251/CL.2024.213.243>
- [11] E. Şakar, Ö. F. Özpolat, B. Alım, M. I. Sayyed, M. Kurudirek, Radiation Physics and Chemistry **166**, 108496 (2020); <https://doi.org/10.1016/j.radphyschem.2019.108496>
- [12] M. I. Sayyed, A. Ibrahim, M. A. Abdo, and M. S. Sadeq, Journal of Alloys and Compounds **904**, 164037 (2022); <https://doi.org/10.1016/j.jallcom.2022.164037>
- [13] R. Iordanova, M. Milanova, A. Yordanova, L. Aleksandrov, N. Nedyalkov, R. Kukeva, P. Petrova, Materials **17**, 1415 (2024); <https://doi.org/10.3390/ma17061415>
- [14] B. Topper, D. Möncke, R. E. Youngman, C. Valvi, E. I. Kamitsos, C. P. E. Varsamis, Physical Chemistry Chemical Physics **25**, 5967–5988 (2023); <https://doi.org/10.1039/d2cp05517a>
- [15] J. Ahlawat, S. Pawaria, N. Deopa, S. Dahiya, R. Punia, A. S. Maan, Applied Physics A **128**, 923 (2022); <https://doi.org/10.1007/s00339-022-05997-w>
- [16] Yu. S. Hordieiev, A. V. Zaichuk, Journal of Ovonic Research **20**(3), 273 (2024); <https://doi.org/10.15251/jor.2024.203.273>
- [17] M. A. Azooz, H. A. ElBatal, Materials Chemistry and Physics **240**, 122129 (2020); <https://doi.org/10.1016/j.matchemphys.2019.122129>
- [18] D. Singh, K. Singh, G. Singh, Journal of Physics: Condensed Matter **20**(7), 075228 (2008); <https://doi.org/10.1088/0953-8984/20/7/075228>
- [19] A. Dietzel, Glasstech Ber. **22**, 41 (1968).
- [20] M. Saad, M. Poulain, Materials Science Forum **19–20**, 11 (1987); <https://doi.org/10.4028/www.scientific.net/msf.19-20.11>
- [21] A. V. Nosenko, Y. S. Hordieiev, V. I. Goleus, Voprosy Khimii i Khimicheskoi Tekhnologii **1**, 87 (2018).
- [22] V. Dimitrov, T. Komatsu, Journal of Chemical Technology and Metallurgy **45**, 219 (2010).
- [23] G. N. Greaves, S. Sen, Adv. Phys. **56**, 1 (2007); <https://doi.org/10.1080/00018730601147426>
- [24] Yu. S. Hordieiev, A. V. Zaichuk, Chalcogenide Letters **19**(12), 891 (2022); <https://doi.org/10.15251/CL.2022.1912.891>
- [25] H. Doweidar, Y. B. Saddeek, Journal of Non-Crystalline Solids **356**, 1452 (2010); <https://doi.org/10.1016/j.jnoncrysol.2010.04.036>
- [26] S. Alomairy, Z. A. Alrowaili, I. Kebaili, E. A. A. Wahab, C. Mutuwong, M. S. Al-Buriah, K. S. Shaaban, Silicon **14**, 5661 (2022); <https://doi.org/10.1007/s12633-021-01347-2>
- [27] N. Alfryyan, A. H. Alomari, Z. A. Alrowaili, H. H. Somaily, I. O. Olarinoye, C. Mutuwong, S. Al-Qais, and M. S. Al-Buriah, Optik **270**, 170050 (2022); <https://doi.org/10.1016/j.ijleo.2022.170050>
- [28] A. M. Babeer, H. Y. Amin, M. I. Sayyed, A. E.-R. Mahmoud, M. S. Sadeq, Optical Materials **149**, 115131 (2024); <https://doi.org/10.1016/j.optmat.2024.115131>
- [29] I. O. Olarinoye, Y. S. Rammah, S. Alraddadi, C. Sriwunkum, A. F. Abd El-Rehim, H. Y. Zahran, M. S. Al-Buriah, Ceramics International **46**, 29191 (2020); <https://doi.org/10.1016/j.ceramint.2020.08.092>
- [30] M. S. Sadeq, M. I. Sayyed, M. A. Abdo, H. E. Ali, A. E.-R. Mahmoud, H. A. Ahmed, Radiation Physics and Chemistry **212**, 111027 (2023); <https://doi.org/10.1016/j.radphyschem.2023.111027>
- [31] G. Lakshminarayana, S. O. Baki, A. Lira, M. I. Sayyed, I. V. Kityk, M. K. Halimah, M. A. Mahdi, Journal of Materials Science **52**, 7394 (2017); <https://doi.org/10.1007/s10853-017-0974-0>
- [32] A. Devidas, T. Sankarappa, A. Malge, M. Heerasingh, J. Pallavi, Bulletin of Materials Science **47**, 240 (2024); <https://doi.org/10.1007/s12034-024-03299-w>
- [33] M. I. Sayyed, M. H. A. Mhareb, M. K. Hamad, Optical Materials **150**, 115237 (2024); <https://doi.org/10.1016/j.optmat.2024.115237>
- [34] A. M. Zayed, A. M. El-Khayatt, K. A. Mahmoud, P. Petrounias, M. A. Masoud, Arabian Journal for Science and Engineering (2024); <https://doi.org/10.1007/s13369-024-09300-2>
- [35] M. I. Sayyed, Hakan Akyildirim, M. S. Al-Buriah, E. Lacomme, R. Ayad, G. Bonvicini, Applied Physics A **126**, 88 (2020); <https://doi.org/10.1007/s00339-019-3265-6>